A constitutive model for various structural steels considering shared hysteretic behaviors

Zhiyang Xie [a], Amit Kanvinde [b], Yiyi Chen [a],*

[a] *State Key Laboratory of Disaster Reduction in Civil Engineering, Tongji University, Shanghai 200092, China*
[b] *Department of Civil and Environmental Engineering, University of California, Davis, CA 95616, USA*

ABSTRACT

A unified constitutive model for structural steels is proposed to reproduce commonly observed hysteretic behaviors that are not represented effectively by current models. This model utilizes a concise description of the Bauschinger effect and a virtual boundary surface to formulate a mathematically improved evolution rule for the hardening behavior in the re-yielding and the subsequent stagnation stage. The model includes an explicit discrete update formulation to describe strain range dependence, in a manner that does not require iterative solution. Based on the existing experimental results, this model considers three cyclic mechanisms resulting in the variation of size of the stress boundary surface in different loading histories. For a better description of cyclic behaviors, two new plastic internal variables are proposed to determine the growth of saturated stress in fixed strain range and its temporary decrease under intermediately reverse deformation. For facilitating calibration, evolution rules for this model are established as set of independent equations that may be calibrated separately. Based on the calibrated parameters, the simulation results of proposed model show remarkable agreement with monotonic as well as cyclic testing data of three different steel grades with various measured strength, particularly in the case of irregular loading histories.

© 2020 Elsevier Ltd. All rights reserved.

1. Introduction

Accurate constitutive models are required to represent the response of structural steels under irregular loading histories similar to those produced by seismic loading. Moreover, in recent years there has been significant development in the area of high performance structural steels, including high-strength steels [1] and low yield point, high ductility steels [2]. Extensive experimental and theoretical investigations have revealed work-hardening modes including cyclic softening that are peculiar to these steels that constitutive models used for conventional steels are unable to capture [3–17]. As a result, a unified constitutive model for all types of structural steels is highly desirable. In this paper, a unified phenomenological constitutive model is proposed on the basis of different hysteretic behaviors that have been reported in literature for various types of steels, as well as those observed in experimental data obtained as part of this study.

The Bauschinger effect is commonly noted in a multitude of cyclic tests on metallic materials, which is characterized by the reduced yield stress after the reverse plastic deformation. In the framework of the classical plasticity, represented by the theories of [18–31], this phenomenon is represented through the yielding function consisting of the backstress as well as the yield stress that indicates the kinematic hardening and the isotropic hardening respectively. Recently, extensive models are developed by incorporating a sophisticated dynamic recovery term in order to produce a better prediction of ratchetting effect [32–47]as well as the hysteric behavior [15,48–50]. In particular, to precisely describe the transient Bauschinger effect and the subsequent work-hardening stagnation, Yoshida and Uemori [16] developed a virtual boundary surface based on the conventional single surface model so that the advantages derived from a conventional Armstrong Frederick (AF) model [19] can be retained together with additional capacities of rigorously depicting the hardening stagnation. Similarly, as reported in the study accomplished by Ohno and Wang [51], the multisurface form of Model II was obtained based on the transformation proposed in the previous study [52], which is similar with the YU model in terms of the evolution rule of backstresses and accordingly shares the advantage of two surface model in prediction of cyclic stress-strain loops. Basically, the transient Bauschinger effect and subsequent work-hardening stagnation can be appropriately incorporated in both models by virtue of the notion of multisurface. With the collective consideration of the advantages and shortcomings of the popular existing models, this study formulates a constitutive model that also overcomes convergence problems along with the advantages in the precise prediction of hysteretic loop.

---

* Corresponding author.
  E-mail address: yiyichen@tongji.edu.cn (Y. Chen).

Furthermore, the memorized strain range dependent hardening stagnation can be regarded as another significant phenomenon, which is characterized by the stabilized hysteresis loop emerging under cyclic loading in fixed memorized strain range. For the description of such behavior, a new plastic internal variable was proposed by Chaboche [28] to memorize the largest plastic strain range in the loading history. Then a generalized formula for the memorization effect based on the notion of non-hardening region developed by Ohno [53].After that, this effect is commonly incorporated in the recently proposed models for the description of the hardening/softening behaviors [15,54–57]. In this paper, the evolution rule of memory surface in strain space is represented by the explicit discrete update formulations to facilitate the numerical procedures.

Recently, in the field of earthquake engineering, accurate assessment of structural response, particularly under irregular loading histories (e.g., those produced by near-fault ground motions) has become an important field of study [58]. Such loading histories are characterized by large deformation pulses at the beginning of the earthquake, which might lead to the incipient large magnitude of plastic deformation followed by subsequent cycles of reduced strain amplitude. Under such conditions, conventional models often grossly misrepresent the degree of stress saturation in subsequent cycles. Additionally, some distinctive hardening behaviors, including the gradual increase of hardening stress in fixed memorized strain range as well as the variation of elastic region with respect to the memorized strain range [5,6,8,9,59], are also incorporated in the proposed model. The evolution rules of these aforementioned effects are formulated by the mutually independent equations with discrete update formulations, which would significantly facilitate the calibration process as well as the numerical iterative procedure.

This paper aims to propose a unified constitutive model that is appropriate to describe the shared cyclic behaviors of different structural steels. Technically given the advantage of the multi-surface model in accurate description of transient Bauschinger effect as well as the strain range dependence, we developed a new form of backstress evolution to improve the accuracy as well as the computational efficiency. Furthermore, based on the existing cyclic testing data, three separated mechanisms have been firstly identified to be the major cause of the variation of the stress boundary surface, and then formulated by corresponding equations. Finally, in order to present the validity of proposed model, total 25 cyclic testing data of three structural steels under regular and irregular loading are selected for the validation of proposed model. Meanwhile, another two conventional models (Chaboche Model and

YU Model) have also be used to examine the shortcomings of previous models so as to demonstrate the improvement resulting from this proposed model.

2. The motivation for the development of the new model

In the field of structural engineering, the Chaboche model [26] is possibly the most commonly used constitutive model employed in the simulation of steel components subjected to the cyclic loading. The popularity of this model may be attributed to its incorporation in popular finite element platforms (e.g., [60]) and its simplicity in terms of the formulations as well as the corresponding numerical methods. For the description of the nonlinear hardening behavior, the Chaboche model incorporates the isotropic term complying with an exponential law and a nonlinear kinematic hardening term that consists of multiple backstresses. These backstresses are defined as the combination of linear hardening as well as nonlinear relaxation term. However, the classical Chaboche model (as originally proposed [26]) considers only the accumulated equivalent plastic strain in its formulation of both the isotropic and kinematic components, and thus does not consider the memory effect which is observed most typically in the multi-level increasing strain amplitude cyclic test. This phenomenon is characterized by the hardening stress being saturated within certain memorized strain range, while the predicted curve generated by the classical Chaboche model (considering only the accumulated strain and disregarding the strain range) approaches the ultimate level prematurely, as illustrated by Fig. 1a. To address this issue, a new plastic internal variable for memorization of the maximum plastic strain was proposed to control the isotropic hardening, as cited in [28].

However, both of the Chaboche models are still unable to produce an accuracy prediction of the stress-strain relationship in the re-yielding stage. To address this issue, the YU model was developed [16], which incorporates the so-called transient Bauschinger effect and subsequent work-hardening stagnation. Unlike conventional multi-surface models, the evolution rule of kinematic hardening is defined as to explicitly determine the saturated stress and the hardening rate in the re-yielding stage, as shown in Fig. 1b. However, the YU models employ a power hardening law (in contrast to the linear rule of the Chaboche model); this is susceptible to numerical problems due to the singularity of derivatives when the power exponent is less than unity. Furthermore, the size of the boundary surface in the YU model evolves with respect to the accumulated plastic strain while the evolution rule of the memory surface determines whether the expansion occurs. This compromises
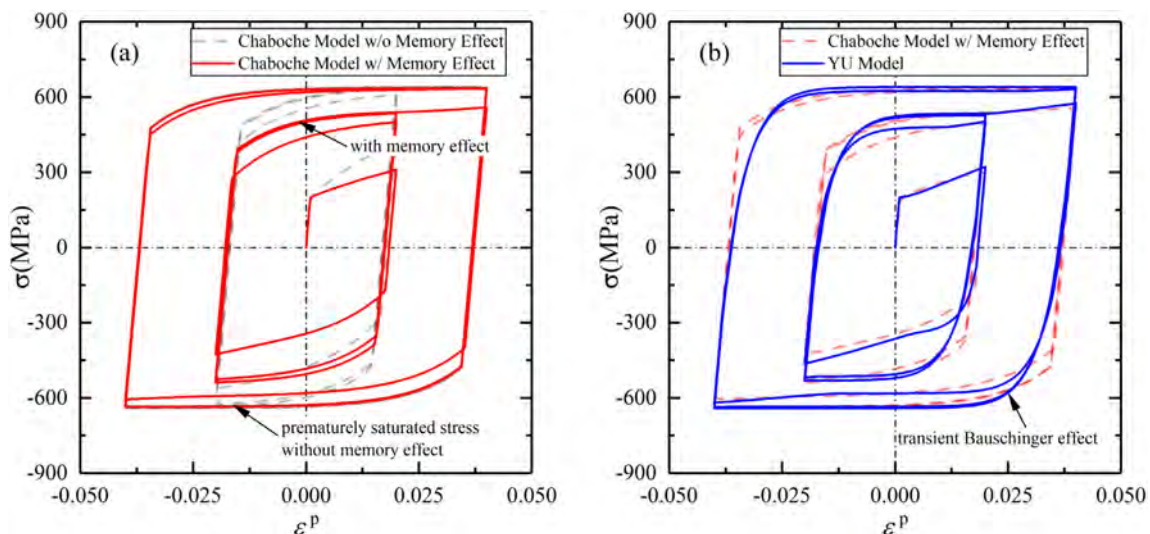
Fig. 1. Typical stress-strain curves based on (a) Chaboche model with/without memory effect and (b) YU model under increasing strain amplitude controlled loading protocol.

accuracy in cases when the expansion rate varies with respect to the memorized plastic strain range in the loading history.

Moreover, the YU model is also unable to reproduce the temporary decrease in saturated stress during smaller strain amplitudes – an important effect that has been noted in common structural steels [5,11,12,15,17]. From the stress-strain response in the multi-level decreasing strain amplitude history, it is concluded that this phenomenon can only be observed when the reverse plastic deformation is applied at the moment when the current plastic strain is considerably less than the maximum of plastic strain range in the loading history. Moreover, the decrease in saturated stress will gradually vanish if the specimen is subjected to the subsequent increasing strain amplitude, which can be referred as to the reversibility of the decrease in saturated stress. The reason why the Chaboche or YU model fail to describe such behavior can be interpreted as the plastic internal variables monotonically increase during the entire loading history. As illustrated in the Fig. 2, these variables, represented by the accumulated plastic strain and the maximum plastic strain, accordingly result in an overestimation of the saturated stress only after a strain larger than subsequent strain cycles is applied.

3. The constitutive model

3.1. Basic framework of the new model

The framework of this constitutive model is established on the classical phenomenological metallic plastic model, where the total strain increment $d\boldsymbol{\varepsilon}$ is decomposed into the elastic strain increment $d\boldsymbol{\varepsilon}^e$ as well as the plastic strain increment $d\boldsymbol{\varepsilon}^p$, as expressed in Eq. (1) and denoted in terms of symmetric tensor with bold letter.

$$d\boldsymbol{\varepsilon} = d\boldsymbol{\varepsilon}^e + d\boldsymbol{\varepsilon}^p \tag{1}$$

The incremental stress may be determined as:

$$d\boldsymbol{\sigma} = \mathbf{C} : d\boldsymbol{\varepsilon}^e \tag{2}$$

where the $\mathbf{C}$ is the elastic moduli assumed as a constant fourth-order symmetric tensor. Furthermore, the evolution of the plastic strain is assumed to comply with the associative flow rule with respect to the yield function, where a generalized form combined with the kinematic and isotropic portions is adopted, as expressed by Eq. (3–5).

$$d\boldsymbol{\varepsilon}^p = dp \cdot \frac{\partial f}{\partial \boldsymbol{\sigma}} \tag{3}$$

$$dp = \sqrt{\frac{2}{3} d\boldsymbol{\varepsilon}^p : d\boldsymbol{\varepsilon}^p} \tag{4}$$

$$f = \sqrt{\frac{3}{2} (\mathbf{S} - \boldsymbol{\alpha}) : (\mathbf{S} - \boldsymbol{\alpha})} - Y \tag{5}$$

where the term $\mathbf{S}$ denotes the stress deviator, variable $\boldsymbol{\alpha}$ denotes the center of the elastic region and the term Y represents its size.

3.2. The mathematically improved description of work-hardening stagnation

Inspired by the YU model, the backstress $\boldsymbol{\alpha}$ is expressed as the summation of the motion of the center of the boundary surface(denoted by $\boldsymbol{\beta}$) and the relative movement of the center of the yield surface(denoted by $\boldsymbol{\alpha}_*$) with respect to $\boldsymbol{\beta}$, as given by Eq. (6).

$$\boldsymbol{\alpha} = \boldsymbol{\beta} + \boldsymbol{\alpha}_* \tag{6}$$

$$\boldsymbol{\beta} = \sum_{i=1}^{ni} \boldsymbol{\beta}^{(i)} \tag{7}$$

$$d\boldsymbol{\beta}^{(i)} = m_\beta^{(i)} \left(\frac{2}{3} b_{sat}^{(i)} \cdot d\boldsymbol{\varepsilon}^p - \boldsymbol{\beta}^{(i)} \cdot dp \right) \tag{8}$$

$$\boldsymbol{\alpha}_* = \sum_{j=1}^{nj} \boldsymbol{\alpha}_*^{(j)} \tag{9}$$

$$d\boldsymbol{\alpha}_*^{(j)} = m_\alpha^{(j)} \left(\frac{2}{3} \omega^{(j)} \cdot a \cdot d\boldsymbol{\varepsilon}^p - \boldsymbol{\alpha}_*^{(j)} \cdot dp \right) \tag{10}$$

$$a = R - Y \tag{11}$$

$$\sum_{j=1}^{nj} \omega^{(j)} = 1.0 \tag{12}$$

In this model, the evolution rules of variables $\boldsymbol{\beta}$ and $\boldsymbol{\alpha}_*$ are formulated by the Eqs. (7) and (9) respectively, based on Chaboche Model
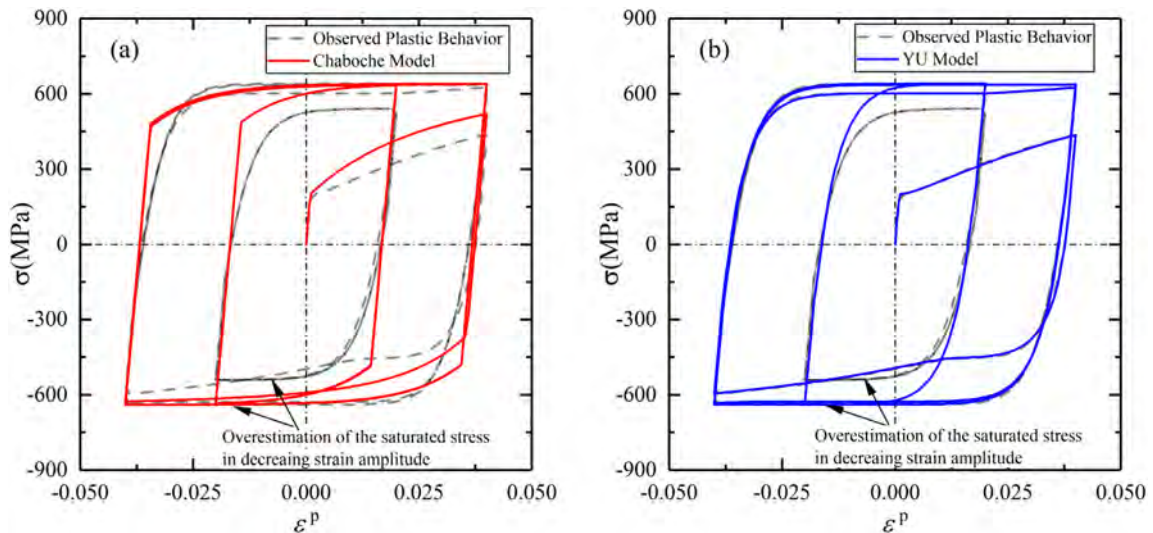
Fig. 2. Typical stress-strain curves based on (a) Chaboche model and (b) YU model compared with commonly observed plastic behavior under decreasing strain amplitude controlled loading protocol.

[26]. These variables are both expressed as the combination of a desired number of sub-components $\boldsymbol{\beta}^{(i)}$ and $\boldsymbol{\alpha}_*^{(i)}$, which comply with similar evolution rule, as given by Eqs. (8) and (10) respectively. The variable a in Eq. (10) is defined as the difference between the radiuses of the boundary (denoted by R) and yield surface (represented by Y), as given by Eq. (11). In addition, the determination of parameters $\omega^{(j)}$ in Eq. (10) shall satisfy the condition prescribed as the Eq. (12). In uniaxial cyclic tension-compression loading scheme, the evolution Eq. (10) is reduced to the one-dimensional formula, as expressed by Eq. (13).

$$d\alpha_*^{(j)} = m_\alpha^{(j)}\left(\omega^{(j)}\cdot a\cdot d\varepsilon^p - \alpha_*^{(j)}\cdot|d\varepsilon^p|\right) \tag{13}$$

This equation yields any individual variable $\alpha_*^{(j)}$ tending to $\omega^{(j)}\cdot a$ or $-\omega^{(j)}\cdot a$ so that their summation α_* will accordingly approach to a or $-a$, constrained by Eq. (12). Therefore, the ultimate saturated stress will tend to $R + \beta$ or $-R + \beta$, in forward or reverse plastic deformation, respectively. As for a general situation in the three-dimensional space, the evolution Eq. (10) combined with the definition in Eq. (11) and constraint in Eq. (12) would eventually lead to such a scenario, as illustrated in Fig. 3, where the yield surface remains inscribed within the enclosure of boundary surface, implying hardening stagnation. By relating the movement and deformation of the boundary surface to specific plastic internal variables, the possible stress state and magnitude is confined within the domain of the boundary surface.

3.3. The discrete update formulation of the memory surface

Based on the experimental investigation on the cyclic behavior of the structural steel, primarily through the researches on the saturated stress within different memorized strain ranges, it is suggested that the hardening stress in stagnation state is dependent on the maximum value of equivalent plastic strain in the entire loading history. In this presented model, we use generalized formulation of memory surface defined in the strain space, proposed by Ohno [53] as expressed by (Eqs. 14–18):

$$g = \sqrt{\frac{2}{3}(\boldsymbol{\varepsilon}^p - \mathbf{q}):(\boldsymbol{\varepsilon}^p - \mathbf{q})} - r \tag{14}$$

$$dr = \begin{cases} h\cdot(\mathbf{n}^p : \mathbf{n}^g)\cdot dp & (g = 0 \text{ and } \mathbf{n}^p : \mathbf{n}^g > 0) \\ 0 & (g < 0 \text{ or } \mathbf{n}^p : \mathbf{n}^g \leq 0) \end{cases} \tag{15}$$

$$d\mathbf{q} = \begin{cases} (1-h)\cdot d\eta\cdot \mathbf{n}^g & (g = 0 \text{ and } \mathbf{n}^p : \mathbf{n}^g > 0) \\ \mathbf{0} & (g < 0 \text{ or } \mathbf{n}^p : \mathbf{n}^g \leq 0) \end{cases} \tag{16}$$

$$\mathbf{n}^p = \frac{d\boldsymbol{\varepsilon}^p}{\sqrt{d\boldsymbol{\varepsilon}^p : d\boldsymbol{\varepsilon}^p}} \tag{17}$$

$$\mathbf{n}^g = \frac{\boldsymbol{\varepsilon}^p - \mathbf{q}}{\sqrt{(\boldsymbol{\varepsilon}^p - \mathbf{q}) : (\boldsymbol{\varepsilon}^p - \mathbf{q})}} \tag{18}$$

Where the equation of the memory surface g is defined as the Eq. (14) and the notation $\mathbf{q}$ and r represent the center as well as the radius of the memory surface, respectively. In the Eq. (15), the term dp represents the increment of the equivalent plastic strain defined as Eq. (4) so that the term $(\mathbf{n}^p : \mathbf{n}^g) \cdot dp$ is equal to the projection of the incremental plastic strain $d\boldsymbol{\varepsilon}^p$ onto the normal direction of the memory surface. Similarly, the term $d\eta$ in Eq. (16) determines the length of the term $d\mathbf{q}$ that can be obtained by the equation of the memory surface, as presented in the following paragraphs in this section. Furthermore, the constant parameter h in Eqs. (15) and (16) determines the evolution rate of the size and center of the memory size.

The next step is to transform those given evolution rules to corresponding iterative update formulas. Through the linearization, the evolutionary path of $\Delta\boldsymbol{\varepsilon}^p$ can be assumed as linear and divided as two separated portions: non-evolution stage indicated by the vector in red color and the successive evolution stage symbolized by the vector in blue color, as illustrated in Fig. 4. Meanwhile, the evolution rule of the center of memory surface can be formulated by the following Eq. (19).

$$\Delta\mathbf{q} = (1-h)\cdot\Delta\eta\cdot\mathbf{n}_{n+1}^g \tag{19}$$

Let the notation $\boldsymbol{\zeta}_{n+1}$ and $\widetilde{\boldsymbol{\zeta}}_{n+1}$ be defined as per Eqs. (20) and (21), respectively

$$\boldsymbol{\zeta}_{n+1} = \boldsymbol{\varepsilon}_{n+1}^p - \mathbf{q}_{n+1} \tag{20}$$

Fig. 3. Schematic illustration of the hardening stagnation governed by the virtual boundary surface in deviatoric stress space.
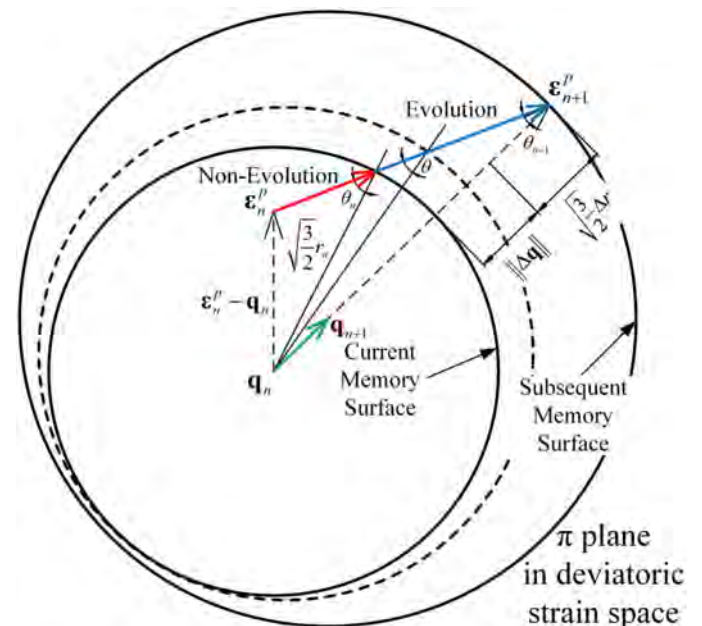
Fig. 4. Schematic diagram of the discrete update formulation of memory surface defined in the deviatoric strain space.

$$\widetilde{\boldsymbol{\zeta}}_{n+1} = \boldsymbol{\varepsilon}^{p}_{n+1} - \mathbf{q}_n \tag{21}$$

By substituting the Eqs. (20, 21) into Eq. (19), the following Eqs. (22), (23) can be obtained.

$$\mathbf{n}^{g}_{n+1} = \widetilde{\mathbf{n}}^{g}_{n+1} = \frac{\boldsymbol{\zeta}_{n+1}}{\|\boldsymbol{\zeta}_{n+1}\|} = \frac{\widetilde{\boldsymbol{\zeta}}_{n+1}}{\|\widetilde{\boldsymbol{\zeta}}_{n+1}\|} \tag{22}$$

$$\|\boldsymbol{\zeta}_{n+1}\| = \|\widetilde{\boldsymbol{\zeta}}_{n+1}\| - (1-h)\cdot\Delta\eta \tag{23}$$

Furthermore, the increment of the radius of memory surface can be obtained by the integral along the linear path of $\Delta\boldsymbol{\varepsilon}^p$, as expressed by Eq. (24).

$$\Delta r = \int dr = \int_{\Delta p_r}^{\Delta p} h\cdot(\mathbf{n}^p : \mathbf{n}^g)\cdot d(\delta p) = h\cdot\left(\sqrt{\frac{2}{3}}\|\widetilde{\boldsymbol{\zeta}}_{n+1}\| - r_n\right) \tag{24}$$

Where the notation δp indicates the variation of the accumulated equivalent plastic strain p from (n-th) to (n + 1-th) step, while the lower bound of the integral denoted by Δp_r is the increment of the accumulated plastic strain within the non-evolution region, as indicated by the red vector in Fig. 4. Furthermore, the evolution rule of the center of memory surface can be formulated by Eq. (25) by substituting the Eqs. (23, (24) into the Eq. (14).

$$\Delta\mathbf{q} = \sqrt{\frac{3}{2}}\cdot(1-h)\cdot\left(\sqrt{\frac{2}{3}}\|\widetilde{\boldsymbol{\zeta}}_{n+1}\| - r_n\right)\cdot\mathbf{n}^{g}_{n+1} \tag{25}$$

Eventually, the complete discrete update formulations of the memory surface evolution can be expressed by Eqs. (27) and (28).

$$g^{\text{trial}}_{n+1} = \sqrt{\frac{2}{3}}\|\widetilde{\boldsymbol{\zeta}}_{n+1}\| - r_n \tag{26}$$

$$\Delta r = h\cdot\langle g^{\text{trial}}_{n+1} \rangle \tag{27}$$

$$\Delta\mathbf{q} = \sqrt{\frac{3}{2}}\cdot(1-h)\cdot\langle g^{\text{trial}}_{n+1} \rangle\cdot\widetilde{\mathbf{n}}^{g}_{n+1} \tag{28}$$

where the notation $\langle\cdot\rangle$ stands for function $\langle x\rangle \equiv \frac{x+|x|}{2}$. Note that the first-order derivative of the function $\langle x\rangle$ is discontinuous at the point $x = 0$, which compromises convergence due to singularity of the derivative. To mitigate this, we employ herein an alternative smooth sigmoid function $S(x)$ to replace the original non-smooth function in the numerical solving process, as given by Eq. (29). Through choosing a suitably large value of the rate factor k, the aforementioned piecewise linear function $\langle x\rangle$ may be approximated by the Eq. (30), which mitigates the convergence problem due to the continuity of its first-order derivative, as shown in Eqs. (31), (32).

$$S(x) = \frac{1}{1 + \exp(-k\cdot x)} \tag{29}$$

$$\langle x\rangle \approx S(x)\cdot x \tag{30}$$

$$S'(x) = k\cdot S(x)\cdot[1 - S(x)] \tag{31}$$

$$\langle x\rangle' \approx S'(x)\cdot x + S(x) \tag{32}$$

Through smoothing the original piecewise linear function, we can obtain a mathematically improved approximation that is compatible with the iterative solving algorithm in the backward-Euler framework, as given by Eqs. (33), (34).

$$\Delta r = h\cdot S\left(g^{\text{trial}}_{n+1}\right)\cdot g^{\text{trial}}_{n+1} \tag{33}$$

$$\Delta\mathbf{q} = \sqrt{\frac{3}{2}}\cdot(1-h)\cdot S\left(g^{\text{trial}}_{n+1}\right)\cdot g^{\text{trial}}_{n+1}\cdot\widetilde{\mathbf{n}}^{g}_{n+1} \tag{34}$$

3.4. The evolution rule of the radius of the boundary surface

3.4.1. The decomposition of the radius of the boundary surface

In this study, we consider three major mechanisms resulting in the change of the radius of the boundary surface, as illustrated in the Fig. 5. Therefore, the radius of the boundary surface (denoted by R) may be expressed as the summation of three mutually independent components, as expressed by Eq. (35).

$$R = R_a + R_p - R_c \tag{35}$$

where the notation R_a symbolizes the initial value of the radius of the boundary surface plus its subsequent expansion due to the amplified memorized plastic strain range and the term R_p denotes the growth of the size of boundary surface with respect to the accumulated equivalent plastic strain in certain fixed memorized plastic strain range. In contrast to the first two terms, the last term R_c represents the temporary contraction of the boundary surface usually observed if the re-yielding occurs at an instant when the current equivalent plastic strain does not reach the memorized plastic strain range in the entire loading history. In order to quantify the memorized plastic strain range in three-dimensional space, the constant parameter h in Eq. (33) and (34) is designated as zero. By this method, the memory surface center is fixed at the origin and the term r accordingly represents the maximum value of the equivalent plastic strain $\max\left(\sqrt{2/3\cdot\boldsymbol{\varepsilon}^p : \boldsymbol{\varepsilon}^p}\right)$ in the entire loading history.

3.4.2. The evolution rule of the gradual boundary surface expansion in fixed memorized plastic strain range

The evolution rule of the boundary surface expansion in fixed memorized strain range is formulated by a function with respect to the accumulated equivalent plastic strain and to the corresponding memorized plastic strain range. Furthermore, this function is of the following property that the value of term R_p should be monotonically increasing along with the increase in accumulated equivalent plastic strain, and ultimately tending to a saturated value dependent on the memorized plastic strain range. Conversely, such expansion will be suppressed if the memorized strain range is increased. To achieve this goal, a new incremental plastic internal variable $d\rho$ is proposed to determine the value of term R_p, as given by the Eq. (36).

$$d\rho = dp - dr \tag{36}$$

Note that the new incremental variable $d\rho$ is equal to the increment of equivalent plastic strain dp when the plastic loading process happens within certain fixed memorized strain range since the term dr vanishes. On the order hand, this variable holds zero in the case of the growth of accumulated plastic strain accompanied by the increase in memorized strain range. By virtue of this variable, the evolution rule of term R_p can be formulated by the following Eqs. (37), (38).

$$dR_p = \frac{k_{Rp}\cdot(R_{pmax} - R_p)}{r}\cdot d\rho \tag{37}$$

$$R_{pmax} = R_{pmax0} + (R_{pmax1} - R_{pmax0})\cdot[1 - \exp(-k_{Rpmax}\cdot r)] \tag{38}$$

Governed by the Eq. (37), the expansion of the radius of the boundary surface within fixed memorized stain range will approach the saturated value R_{pmax} in a rate controlled by the material constant k_{Rp}. Additionally, an exponential law is hereby used to describe the relationship between the saturated value R_{pmax} and specific memorized strain range.

a) Mechanism I: the growth of radius of boundary surface due to increase in size of memory surface

b) Mechanism II: the expansion of boundary surface with respect to the increasing accumulated equivalent plastic strain in fixed memory surface

c) Mechanism III: the temporary contraction of boundary surface after intermediately reverse plastic strain applied
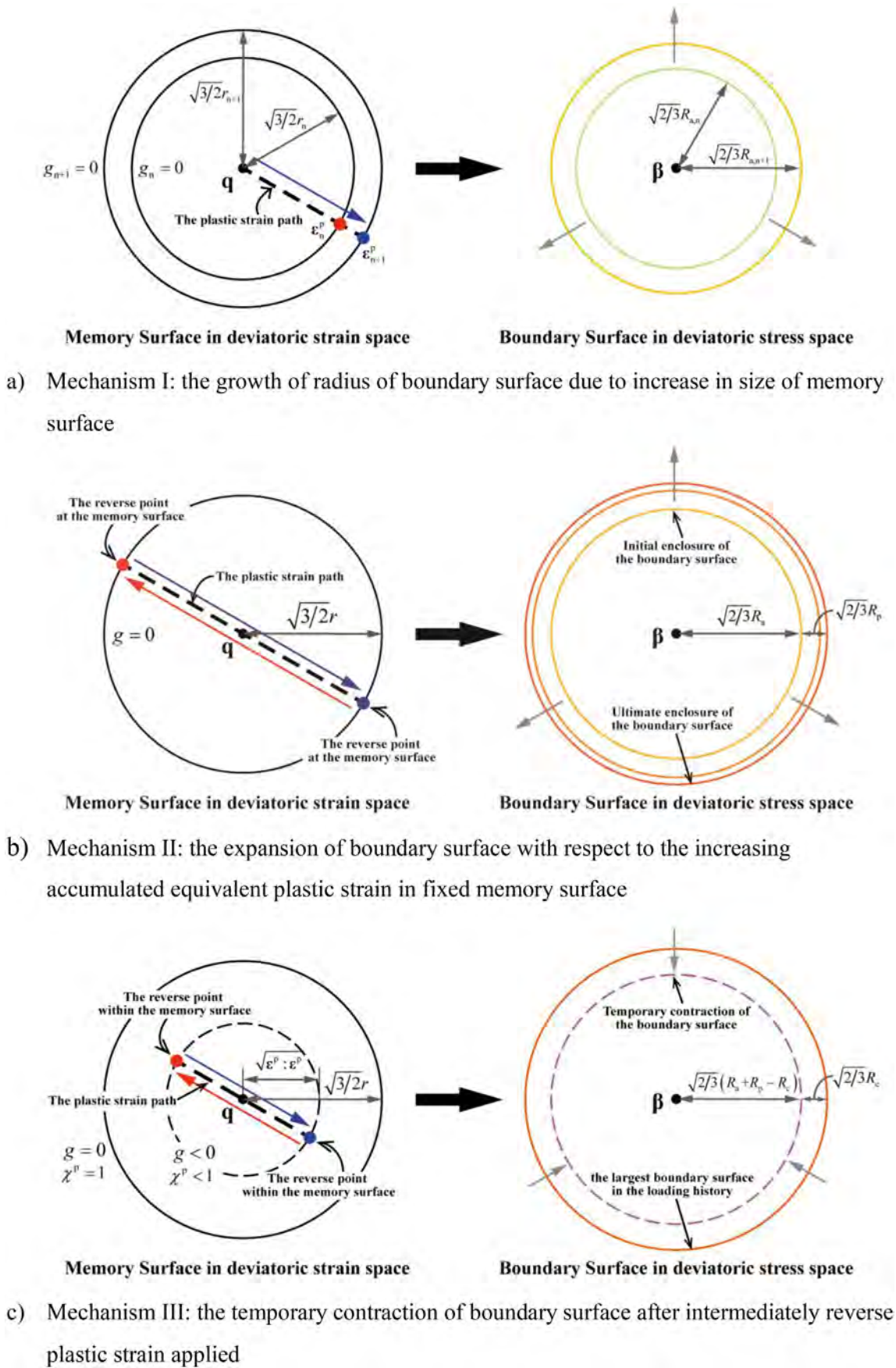
Fig. 5. Schematic diagram of three major mechanisms related to the change of radius of boundary surface.

3.4.3. The evolution rule of temporary contraction of boundary surface due to intermediately reverse plastic deformation

In the conventional plasticity model, this phenomenon might not be accurately depicted since the plastic internal variables, commonly represented by the accumulated equivalent plastic strain (denoted by p) and the memorized plastic strain range (symbolized by r), are monotonically increasing along with the plastic evolution. To address this issue, in this study, a new plastic internal variable (denoted by χ^p) is proposed to indicate the current plastic status, which is defined as the ratio of current equivalent plastic strain to the memorized plastic strain range, as expressed by Eq. (39).

$$\chi^p = \frac{\sqrt{2/3 \cdot \boldsymbol{\varepsilon}^p : \boldsymbol{\varepsilon}^p}}{r} \tag{39}$$

According to its definition, the term χ^p is a normalized variable whose range is the bounded interval $[0, 1]$. Therefore, the condition that its value equals unity indicates that the current plastic point is located on the memory surface and the contraction of the boundary surface does not occur when the reverse displacement is applied.

On the basis of aforementioned introduction, it is summarized that this phenomenon occurs at the beginning of the reverse plastic deformation. In this model, the inner product of two unit direction tensors, denoting the direction of previous as well as current plastic strain increments, is employed to generalize the notion of reverse deformation in uniaxial loading and quantify the difference of loading direction between two successive steps in three-dimensional space, defined as the following Eqs. (40), (41).

$$\mathbf{n}_n^p = \frac{\Delta \boldsymbol{\varepsilon}_n^p}{\|\Delta \boldsymbol{\varepsilon}_n^p\|}, \mathbf{n}^p = \frac{\Delta \boldsymbol{\varepsilon}^p}{\|\Delta \boldsymbol{\varepsilon}^p\|} \tag{40}$$

$$l^p = \mathbf{n}_n^p : \mathbf{n}^p \tag{41}$$

The variable l^p is the cosine of the angle between two successive plastic strain increments. In three-dimensional space, the value of term l^p equals to unity refers to the completely forward plastic deformation.

Then the term R_{ctem} is defined by the Eq. (42) to describe the dependence of contraction of boundary surface on the above newly defined variable χ^p as well as the memorized plastic strain range (denoted by r).

$$R_{ctem} = R_{cmax} \cdot [1 - \exp(-k_{Rc} \cdot r)] \cdot (1 - S_\chi) \tag{42}$$

where the material parameter R_{cmax} symbolizes the ultimate value of the contraction when the memorized plastic strain range tends to infinite, and the constant k_{Rc} determines its evolution rate with respect to the memorized plastic strain range. In addition, another term S_χ is adopted to describes the relationship between the contraction of boundary surface and the current plastic status, as given by Eq. (43).

$$S_{\chi 0} = -\frac{1}{1 + \exp[b_\chi \cdot k_\chi]}$$

$$S_{\chi 1} = 1 - \frac{1}{1 + \exp[-(1 - b_\chi) \cdot k_\chi]} \tag{43}$$

$$S_\chi = \frac{1}{1 + \exp[-(\chi^p - b_\chi) \cdot k_\chi]} + (S_{\chi 1} - S_{\chi 0}) \cdot \chi^p + S_{\chi 0}$$

Eventually, the term R_c, denoting the magnitude of the contraction of the boundary surface, can be expressed by the Eq. (44).

$$R_{c,n+1} = R_{c,n} + (R_{ctem} - R_{c,n}) \cdot \frac{1 - l^p}{2} \tag{44}$$

To illustrate its evolutionary pattern in accordance with these above-mentioned formulas, the following schematic Fig. 6 manifests a typical stress-strain response of a simulated specimen undergoing one

cycle of deformation with a relatively large strain range and then followed by a smaller strain amplitude. Eventually, additional cyclic deformation with a resumed strain amplitude is applied to demonstrate the reversibility of this phenomenon. It is noted that at the first and second reverse deformation point in the large strain range, the terms R_c remains zero since the current equivalent plastic strain equals the memorized plastic strain range, as represented by term $\chi^p = 1$, which will cause term $1 - S_\chi$ being equal to zero and indicate no contraction of boundary surface. During the forward as well as reverse deformation stage after above mentioned turning point, the term R_c holds zero, notwithstanding the variation of term R_{ctem} with respect to the plastic internal variable χ^p. After the hardening stagnation appears significantly, smaller strain amplitude is applied up to approach the subsequent stagnation status. It is showed that the saturated stress is reduced to a lower level, which is determined by substituting term R_{ctem} into the Eq. (44). Eventually, the last cyclic loading with the strain amplitude recovered to the initial value is applied to demonstrate the reversibility of the contraction of boundary surface. At the onset of the last cycle, the value of term R_{ctem} is reset as zero so that the contraction of boundary vanishes since the value of term R_c is updated to zero in accordance with Eq. (44).

3.4.4. Additional consideration of the reduced hardening rate in re-yielding stage following intermediately reverse plastic deformation

Another possibly reasonable explanation for the contraction of boundary surface may be interpreted as that the hardening rate in re-yielding stage is diminished after applying the reverse displacement in an intermediate plastic status. To consider this alternative effect on the reduction of boundary surface, a factor φ for adjusting the hardening rate in re-yielding stage is proposed, as defined by Eq. (45).

$$\varphi = \varphi_{min} + (1 - \varphi_{min}) \cdot S_\varphi \tag{45}$$

where the material parameter φ_{min} represents the minimum value of the reduction factor. Similar with the above section, the herein presented variable S_φ is defined by the following Eq. (46).
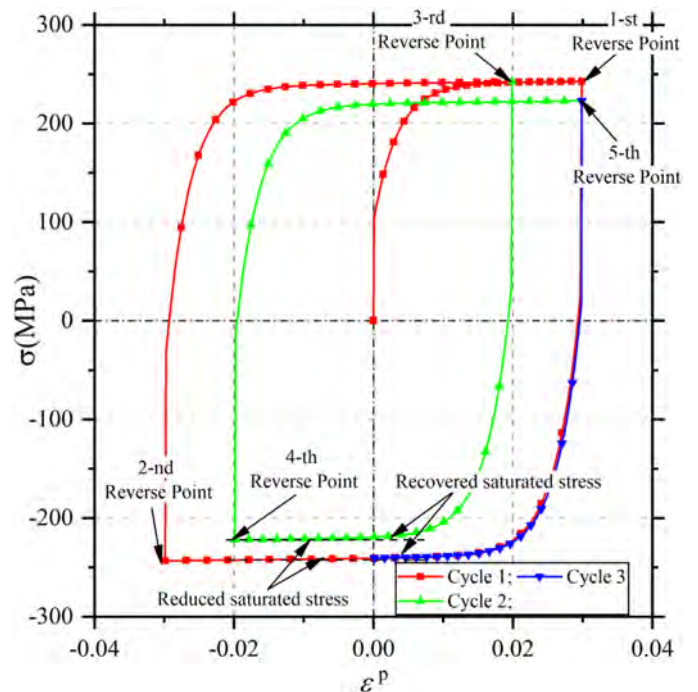
Fig. 6. Schematic illustration of the temporary contraction of boundary surface due to intermediately reverse plastic deformation.

$$S_{\varphi 0} = -\frac{1}{1 + \exp\left[b_\varphi \cdot k_\varphi\right]}$$

$$S_{\varphi 1} = 1 - \frac{1}{1 + \exp\left[-(1-b_\varphi)\cdot k_\varphi\right]} \tag{46}$$

$$S_\varphi = \frac{1}{1 + \exp\left[-(\chi^p - b_\varphi)\cdot k_\varphi\right]} + (S_{\varphi 1} - S_{\varphi 0})\cdot \chi^p + S_{\varphi 0}$$

By substituting the variable φ into Eq. (10), we can obtain a modified variables $\boldsymbol{\alpha}_*^{(j)}$ with the additional consideration of the potential reduction effect on the hardening rate in re-yielding stage, as given by Eq. (47).

$$d\boldsymbol{\alpha}_*^{(j)} = \varphi \cdot m_\alpha^{(j)} \left(\frac{2}{3} \omega^{(j)} \cdot a \cdot d\boldsymbol{\varepsilon}^p - \boldsymbol{\alpha}_*^{(j)} \cdot dp \right) \tag{47}$$

3.4.5. The evolution rule of the amplified memorized strain range induced boundary surface expansion

On the basis of the already-proposed update procedures of term R_p and R_c, the evolution rule of the amplified memorized strain range induced boundary surface expansion can be uniquely determined by the uniaxial stress-strain relationship, as elaborated in the following statements.

In the monotonic tensile loading scheme, it can be readily confirmed that the following equation holds true all through the loading procedure, as expressed by Eq. (48).

$$\Delta \varepsilon_{11}^p = \Delta p = \Delta r \tag{48}$$

Consequently, the term R_p and R_c vanish since the condition in which the accumulated plastic strain equals the memorized plastic strain range eliminates the subsequent increment of the term R_p, and meanwhile the continuously forward plastic deformation, indicating the term l^p holds one, leads to the value of term R_c holding its initial value as zero. Therefore, the magnitude of the boundary expansion can be exclusively determined by the term R_a, as given by Eq. (49).

$$R_{n+1} = R_{a,n+1} \tag{49}$$

Furthermore, in this circumstance, the yield function in three-dimensional space can be reduced to the specific update formulation, as expressed by Eq. (50).

$$\overline{\sigma}_{n+1} = \overline{\alpha}_{n+1} + Y = \sum_{i=1}^{ni} \overline{\beta}_{n+1}^{(i)} + \sum_{j=1}^{nj} \overline{\alpha}_{*,n+1}^{(j)} + Y \tag{50}$$

where the term $\overline{\beta}^{(i)}$ and $\overline{\alpha}_*^{(j)}$ represent the equivalent stress of term $\boldsymbol{\beta}^{(i)}$ as well as $\boldsymbol{\alpha}_*^{(j)}$ in one-dimensional space, respectively, so that their update formulation can be attained based on the evolution rule in three-dimensional space, as given by Eqs. (51), (52).

$$\overline{\beta}_{n+1}^{(i)} = \frac{\overline{\beta}_n^{(i)} + m_\beta^{(i)} \cdot b_{sat}^{(i)} \cdot \Delta r}{1 + m_\beta^{(i)} \cdot \Delta r} \tag{51}$$

$$\overline{\alpha}_{*,n+1}^{(j)} = \frac{\overline{\alpha}_{*,n}^{(j)} + m_\alpha^{(j)} \cdot \omega^{(j)} \cdot a_{n+1} \cdot \Delta r}{1 + m_\alpha^{(j)} \cdot \Delta r} \tag{52}$$

Remark that the terms involved with the accumulated equivalent plastic strain increment Δp and plastic strain increment $\Delta \varepsilon_{11}^p$ are both substituted by the increment of memorized plastic strain range Δr, in accordance with the Eq. (48). Moreover, it is noted that the variable χ^p for current plastic status remain one so that the decrease in re-yielding rate can be excluded from the evolution rule of the term $\overline{\alpha}_*^{(j)}$ through removal of term φ.

By substituting the Eqs. (51) and (52) into Eq. (50) and arrangement, the update formulation of term $R_{a,\ n+1}$ can be obtained, as expressed by Eq. (53).

$$R_a = \frac{\overline{\sigma}(r_{n+1}) - Y - \sum_{i=1}^{ni} \frac{\overline{\beta}_n^{(i)} + m_\beta^{(i)} \cdot b_{sat}^{(i)} \cdot \Delta r}{1 + m_\beta^{(i)} \cdot \Delta r} - \sum_{j=1}^{nj} \frac{\overline{\alpha}_{*,n}^{(j)}}{1 + m_\alpha^{(j)} \cdot \Delta r}}{\sum_{j=1}^{nj} \frac{m_\alpha^{(j)} \cdot \omega^{(j)} \cdot \Delta r}{1 + m_\alpha^{(j)} \cdot \Delta r}} + Y \tag{53}$$

It is concluded that the value of the term R_a can be directly obtained through the results of uniaxial tensile test. Moreover, any monotonically increasing function for the description of the uniaxial stress-strain relationship can be employed theoretically in this framework. To consider collectively the yield plateau and subsequent nonlinear hardening, in this study, the following piecewise function is utilized to depict the aforementioned phenomena, as given by Eq. (54).

$$\overline{\sigma}(r) = \begin{cases} \dfrac{Y_0}{1 - Y_0/E} \cdot (1+r) & (r < \varepsilon_{nh}) \\[2ex] \overline{\sigma}_{nh} + \Delta\overline{\sigma}_{nh} \cdot \{1 - \exp\left[-k_{nh}\cdot(r-\varepsilon_{nh})\right]\} + k_0 \cdot (r-\varepsilon_{nh}) & (r \geq \varepsilon_{nh}) \end{cases} \tag{54}$$

where the parameter ε_{nh} and $\overline{\sigma}_{nh}$ denote the plastic strain range as well as the uniaxial true stress at the end of yield plateau, respectively. The first portion of Eq. (54) is to describe the true stress-logarithmic plastic strain relationship in yield plateau, which is derived from the definition of yield plateau. By substituting the parameter ε_{nh} into this formula, the term $\overline{\sigma}_{nh}$ can be readily determined. As for the second part of Eq. (54), the parameter $\Delta\overline{\sigma}_{nh}$ represents the ultimate increase in the nonlinear hardening stress, while the factor k_{nh} controls the evolutionary rate. In addition, the accompanying linear hardening term (denoted by $k_0 \cdot (r - \varepsilon_{nh})$) is also included herein and governed by linear hardening factor k_0.

3.5. The modified evolution rule of the elastic region based on the original YU model

Based on the investigations conducted by [8,9] on the structural steel, it is suggested that the size of elastic region is usually dependent on the memorized plastic strain range. To take this effect in account, the formula for the evolution of elastic region is proposed as the following Eq. (55).

$$Y = Y_0 - Y_0 \cdot (1 - \varphi_Y) \cdot [1 - \exp(-k_Y \cdot r)] \tag{55}$$

where the material parameter Y_0 symbolizes the initial yield stress and the factor φ_Y indicates the ratio of the ultimate size of elastic region to the initial one. Furthermore, the rate of this process is dependent on the rate factor k_Y.

4. Validation of proposed model based on the material testing data of three types of structural steels

4.1. Outlines of material testing on structural steels

To demonstrate the validity of this model in the prediction of stress-strain relationship under regular as well as irregular actions, the material testing data of three types of structural steels, with Chinese steel grades of LYP100, Q345 and Q420 (equivalent to the S355JR and S420N in EN 10025) respectively, are used as the basis of the following calibration of model parameters and validation of new model. These three involved steels, whose measured yield strength are 104 MPa, 335 MPa and 515Mpa, represent the low yield point steel, the mild steel as well as the high strength steel respectively, which are commonly manufactured and employed in the Chinese civil engineering.

The original experimental data are cited in the two publications accomplished by Zhou [17] and He [5], who conduct the material testing of Q345/Q420 and LYP100 respectively under different cyclic loading protocols. As illustrated in Fig. 7, in these experimental studies, two different specimen configurations are employed in the monotonic and cyclic tests. The overall information of the loading schemes is presented in Table 1 for Q345/Q420 and Table 2 for LYP100, respectively. As illustrated in Figs. 8 and 9, we select five loading protocols for Q345 and Q420 as well as three loading protocols for LYP100 as the representative examples to demonstrate the accuracy of the new model compared with the Chaboche and YU model.

(a) Zhou et al., 2015; (b) He et al., 2019.

4.2. Procedures of parameter calibration based on the characteristics of proposed model

By virtue of the characteristics of the proposed model, the entire material parameters are categorized into three separate groups, in which

Table 2
Loading schemes used in the material testing on LYP100.

Name	Description	Detailed loading schemes (Notation - LS: logarithmic strain; C: Cycles)
SP-00	Monotonic tension	Monotonic tensile loading until ultimate fracture
SP-01	Multi-Level Increasing Strain–Amplitude	LS:±0.02(5C) → LS:±0.04(5C) → LS:±0.06 (3C)
SP-02	Multi-Level Decreasing Strain-Amplitude	LS:±0.08(3C) → LS:±0.06(5C) → LS:±0.04 (5C) → LS:±0.02(5C)
SP-03	Cyclic Loading in 2% Strain-Range	LS: ±0.02 → stagnation status
SP-04	Cyclic Loading in 4% Strain-Range	LS: ±0.04 → stagnation status
SP-05	Cyclic Loading in 6% Strain-Range	LS: ±0.06 → stagnation status
SP-06	Cyclic Loading in 8% Strain-Range	LS: ±0.08 → stagnation status
SP-07	Increasing Strain-Amplitude per Cycle	Increasing 0.5% strain-amplitude per cycle from 0.5% to 6.5%
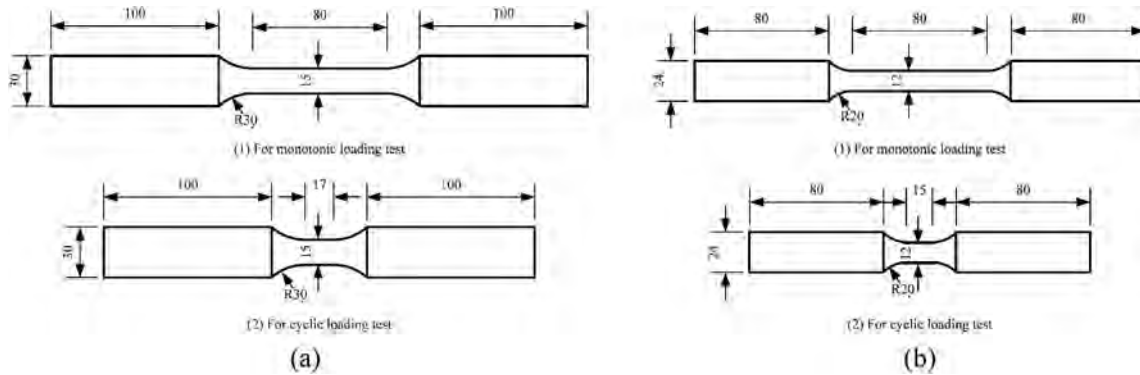
Fig. 7. The specimens for the monotonic and cyclic loading tests conducted by.

Table 1
Loading schemes used in the material testing on Q345/Q420.

Name	Description	Detailed loading schemes (Notation - NS: nominal strain; C: Cycles)
SP-00	Monotonic tension	Monotonic tensile loading until ultimate fracture
SP-01	Multi-Level Increasing Strain–Amplitude	NS:±0.025(5C) → NS:±0.05(5C) → NS:±0.075(5C) → NS:±0.10(5C)
SP-02	Multi-Level Decreasing Strain-Amplitude	NS:±0.10(5C) → NS:±0.075(5C) → NS:±0.05(5C) → NS:±0.025(5C)
SP-03	Tension-Unload	NS:0.01-Unload(5C) → NS:0.02-Unload(5C) → NS:0.04-Unload(5C) → NS:0.06-Unload (5C) → NS:0.08-Unload(5C) → NS:0.10-Unload(5C)
SP-04	Alternant Strain-Amplitude	NS:±0.025(5C) → NS:±0.05(5C) → NS:±0.05(5C) → NS:±0.10(5C)
SP-05	Cumulated Maximum Strain-Range Followed by Increasing Strain-Amplitude: Case I	NS:±0.10(12C) → NS:±0.025(5C) → NS:±0.05(5C) → NS:±0.075(5C) → NS:±0.10(5C) (Note: these loading protocols with underline are not completely applied due to premature ductile fracture)
SP-06	Cumulated Maximum Strain-Range Followed by Increasing Strain-Amplitude: Case II	NS:±0.10(6C) → NS:±0.025(5C) → NS:±0.05(5C) → NS:±0.075(5C) → NS:±0.10(5C)
SP-07	Half-Cycle Maximum Strain-Range Followed by Increasing Strain-Amplitude: Case I	NS:+0.10(0.5C) → NS:±0.025(5C) → NS:±0.05(5C) → NS:±0.075(5C) → NS:±0.10(5C)
SP-08	Half-Cycle Maximum Strain-Range Followed by Increasing Strain-Amplitude: Case II	NS:+0.15(0.5C) → NS:±0.025(5C) → NS:±0.05(5C) → NS:±0.075(5C) → NS:±0.10(5C)
SP-09	Random	As elaborated in the following Table 1b

(a) Strain-amplitudes in random loading scheme

Sequence Number	1	2	3	4	5	6	7	8	9	10	11	12	13	14	15
Strain-Amplitude(%)	−3	+7	−5	+3	−1	+6	−1	+1	−1	+1	−5	+2	−1	+10	−3
Sequence Number	16	17	18	19	20	21	22	23	24	25	26	27	28	29	30
Strain-Amplitude(%)	+2	−6	+5	−2	−1	−3	+3	0	+6	0	+10	−6	+10	−10	+9
Sequence Number	31	32	33	34	35	36	37	38	39	40	41	42	43	44	45
Strain-Amplitude(%)	−10	+1	−10	+1	−5	+3	−2	+7	+1	10	−7	+3	−7	−1	−3
Sequence Number	46	47	48	49	50	51	52	53	54	55	56	57	58		
Strain-Amplitude(%)	+3	−1	+7	−1	+10	−6	−2	−10	+3	−10	+1	−2	0		
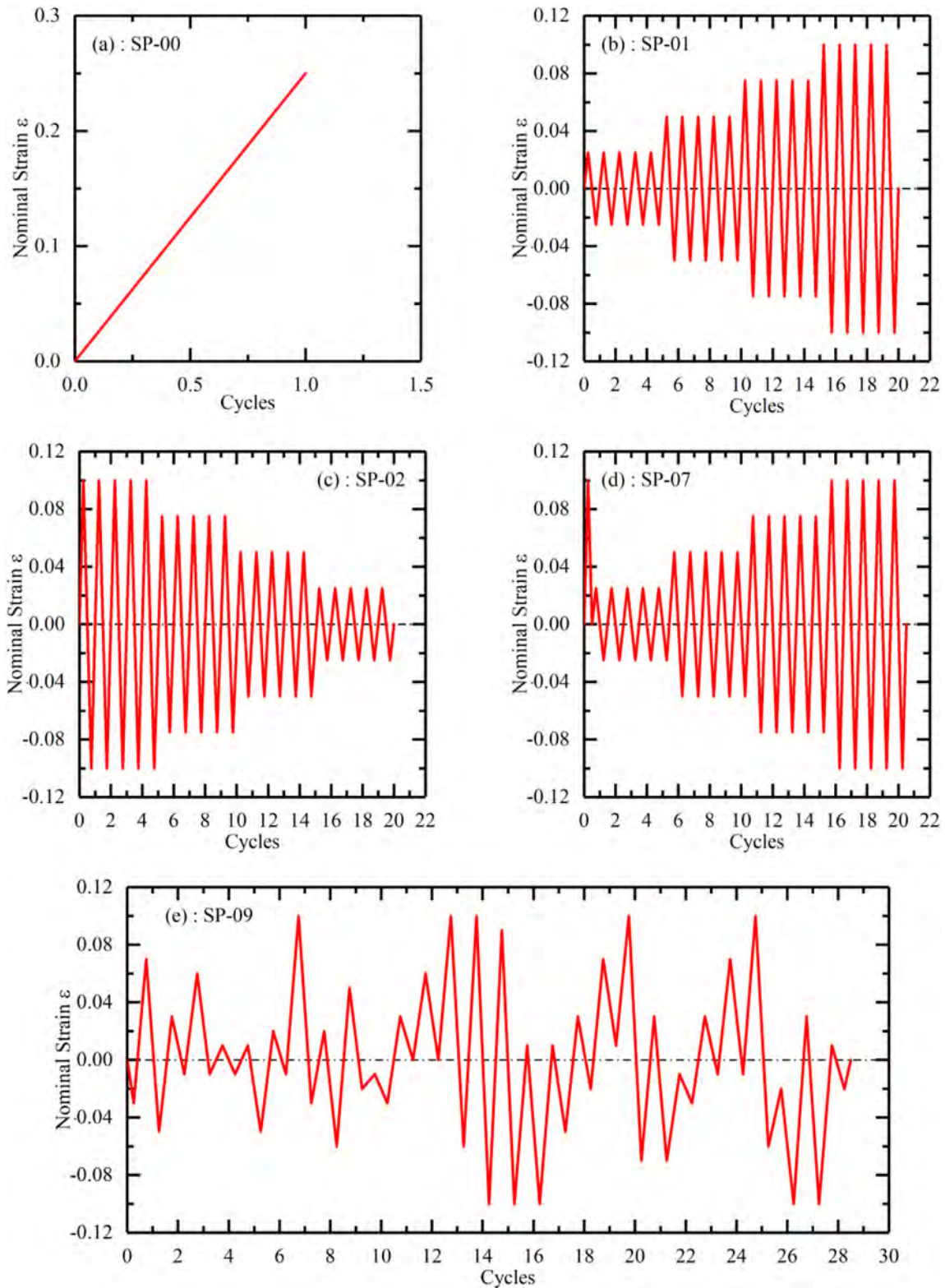
Fig. 8. The selected loading protocols to demonstrate the prediction results of various plastic behaviors in material testing on Q345 and Q420 steels.

the parameters can be calibrated by the monotonic as well as two cyclic materials testing data, respectively. First, based on the monotonic tensile testing data, we can directly obtain the parameters of the first part of the piecewise function [54], including initial yield stress Y_0 and Young's modulus E. For the parameters in nonlinear hardening stage,

the fitting algorithm in MATLAB CurveFitting Tool can be utilized to acquire the approximate material parameters $\Delta\overline{\sigma}_{nh}, k_{nh}, k_0$.

For the parameters that describe cyclic behaviors, they can also be assigned into six categories that are corresponding to specific behaviors possibly emerging in different cyclic loading schemes. The entire
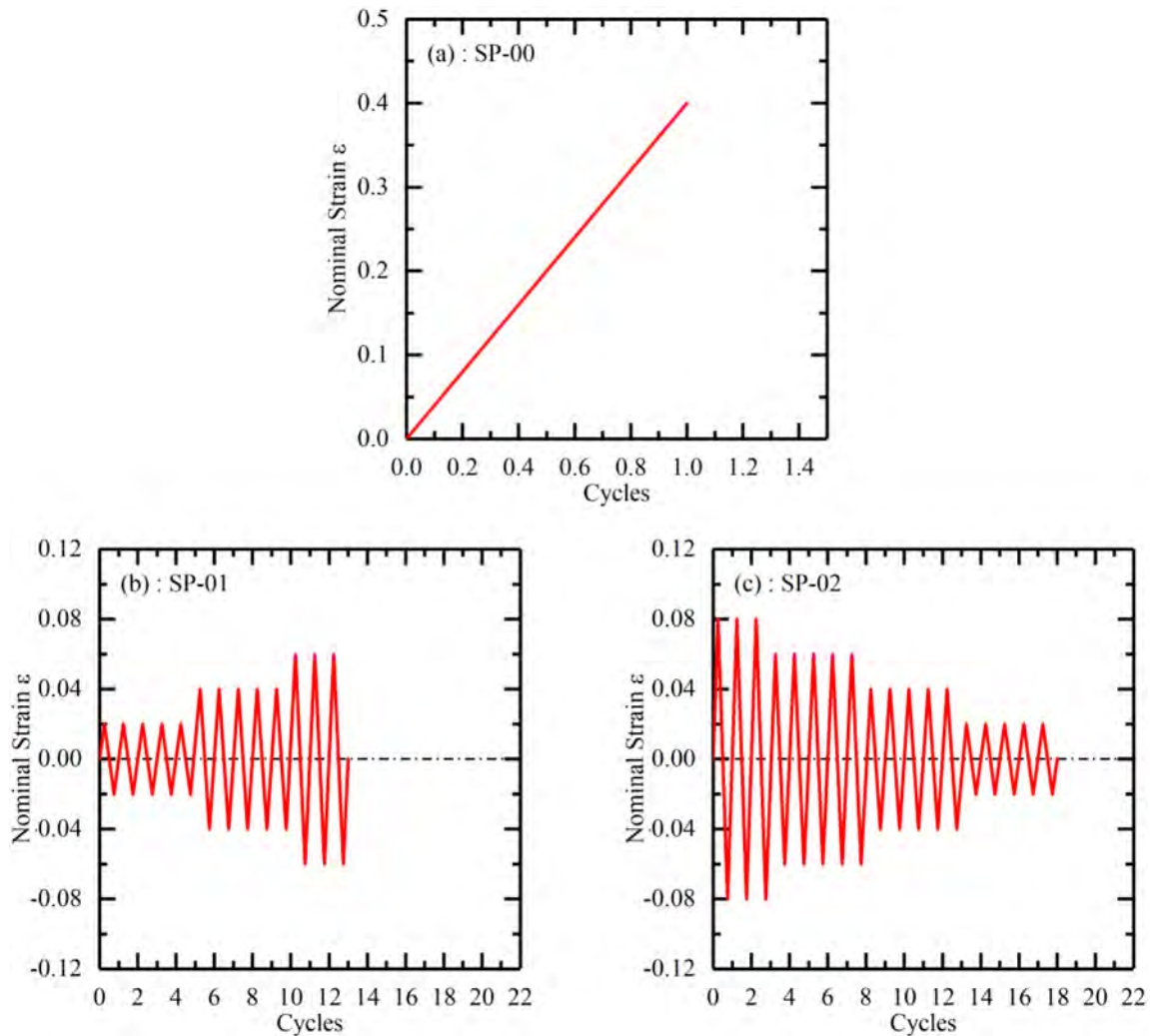
Fig. 9. The selected loading protocols to demonstrate the prediction results of various plastic behaviors in material testing on LYP100 steel.

parameters in the cyclic behavior group can be completely determined by two types of cyclic loading scheme: the multi-level increasing strain amplitude as well as multi-level decreasing strain amplitude controlled loading protocols. To obtain these parameters efficiently, the numerical optimization method built in the MATLAB optimization toolbox and the corresponding procedure proposed by He [5] are implemented to acquire the best approximation.

Remark that the mutual independence of parameters affiliated in different categories plays a significant role in acquiring a reasonable result efficiently. It requires that any individual parameter should be designated to single hardening behavior and there is no significant interaction between the formulas related to different phenomena. In this way, the determination of a specific parameter may not impose distinctive influence on the other parts of the model that are already determined by previously calibrated parameters, which can greatly facilitate the calibration procedure. For instance, in this model, there is inherent mutual independence between the portions involved with monotonic and cyclic behaviors. It means that the simulation result of monotonic tensile testing will not be changed once the corresponding parameters are calibrated by experimental data, no matter how the other parameters for cyclic behaviors are manipulated in the following calibration procedure.

The integrated calibrated parameters are listed in following Table 3, where all parameters are calibrated on the basis of the experimental data from the uniaxial monotonic tensile test, the multi-level increasing

as well as decreasing strain amplitude controlled test. The rest of testing data could be used to validate the capacities of the proposed model in predicting the stress-strain response under the complex seismic actions. Additionally, the aforementioned YU model as well as the conventional Chaboche model are simultaneously utilized to predict the hysteretic response following the identical calibration procedure. The calibrated parameters for these two models are also listed in Table 4 for the YU model as well as Table 5 for the Chaboche Model, respectively. The simulation results based on these two existing models could emphasize the improvement of the prediction contributing to the implementation of the proposed model.

4.3. The validation of proposed model and the comparison with two existing models

The following Figs. 10-12 demonstrate the true stress versus logarithmic strain curves obtained by the implementation of the proposed model, the YU model and the Chaboche model, which are involved with the aforementioned representative loading protocols. By the comparisons with the experimental data, the remarkable agreement with the testing results confirms that the proposed model is appropriate to obtain the stress-strain response for different steel grades under irregular actions. The simulation results of the monotonic tensile tests on three types of structural steels with low, medium as well as high measured yield strength indicate that the initial yield strength and successive hardening

Table 3
Calibrated parameters of proposed model for three steel grades.

Category	Description	Notation	Calibrated parameters for LYP100	Calibrated parameters for Q345	Calibrated parameters for Q420
(a) Parameters calibrated by the data from increasing strain amplitude controlled test.					
Elasticity	Young's modulus	E(MPa)	180,000	205,000	206,000
	Poisson's ratio	ν	0.3	0.3	0.3
Yield plateau	Initial yield stress	Y_0(MPa)	104	335	515
Nonlinear hardening	Plastic strain at the onset of nonlinear hardening	ε_{nh}	0	0.0076	0.0116
	Maximum increase in nonlinear hardening	$\Delta\overline{\sigma}_{nh}$	183.2	197.2	126.8
	Rate factor	k_{nh}	13.47	24.66	25.22
	Linear hardening rate factor	k_0	152.7	446.9	318

Category	Description	Notation	Calibrated parameters for LYP100	Calibrated parameters for Q345	Calibrated parameters for Q420
(b) Parameters calibrated by the data from increasing strain amplitude controlled test.					
Elastic region	Reduced Factor	φ_Y	1.1	0.8	0.5
	Rate factor	k_Y	378.0	66.8	39.2
Center of boundary surface	Rate factors	$m_\beta^{(1)}$	0.19	0.16	0.13
		$m_\beta^{(2)}$	141.21	41.76	51.78
	Saturated values	$b_{sat}^{(1)}$(MPa)	766.98	2495.73	2533.11
		$b_{sat}^{(2)}$(MPa)	0.00	60.72	31.45
Hardening rate in re-yielding stage	Rate factors	$m_\alpha^{(1)}$	200.52	173.94	1619.12
		$m_\alpha^{(2)}$	11,859.18	622.19	374.73
		$m_\alpha^{(3)}$	1183.57	0.0917	153.73
	Proportionality Coefficients	$\omega^{(1)}$	0.250	0.137	0.519
		$\omega^{(2)}$	0.267	0.465	0.278
		$\omega^{(3)}$	0.483	0.398	0.203
Expansion of boundary surface in fixed strain range	Rate factor for hardening	k_{Rp}	0.54	0.77	280
	Initial value	R_{pmax0} (MPa)	0	89.88	0
	Ultimate value	R_{pmax1} (MPa)	130.04	1599.67	497.10
	Rate factor	k_{Rpmax}	84.08	0.467	0.568
(c) Parameters calibrated by the data from decreasing strain amplitude controlled test					
Contraction of boundary surface	Rate factor	k_χ	2.071	3.344	2.482
	Bias	b_χ	0.806	0.812	0.807
	Maximum value	R_{cmax} (MPa)	126.43	270.25	75.96
	Rate factor	k_{Rc}	8.65	5.13	18.03
Reduced hardening rate in re-yielding stage	Rate factor	k_φ	20	19.97	217.40
	Bias	b_φ	0.8	0.925	0.983
	Minimum value	φ_{min}	0.7	0.958	1

Table 4
Calibrated parameters of YU model for three steel grades.

Description	Notation	Calibrated parameters for LYP100	Calibrated parameters for Q345	Calibrated parameters for Q420
Young's modulus	E(MPa)	180,000	205,000	206,000
Poisson's ratio	ν	0.3	0.3	0.3
Initial yield stress	Y_0(MPa)	104	335	515
Re-yielding rate coefficient	C	1903.63	508.01	86.58
Re-yielding rate exponent	γ	0.11	0.22	0.56
Initial size	B(MPa)	119.3	337.96	528.9
Maximum expansion	R_{sat}(MPa)	219.51	246.51	103.24
Rate factor of expansion	m_R	9.94	15.59	50.72
Maximum distance	b_{sat}(MPa)	0.14	2495	2533
Rate factor	m_b	7.4	0.156	0.13
Proportionality coefficient	h	0.2	0.5	1
Initial size of the memory surface	r_0(MPa)	0	0.03	2.85

Table 5
Calibrated parameters of Chaboche model for three steel grades.

Description	Notation	Calibrated parameters for LYP100	Calibrated parameters for Q345	Calibrated parameters for Q420
Young's modulus	E(MPa)	180,000	205,000	206,000
Poisson's ratio	ν	0.3	0.3	0.3
Initial yield stress	Y_0(MPa)	104	335	515
Maximum of the isotropic hardening	Y_{sat}(MPa)	300.91	513.955	571.41
Rate factor of the isotropic hardening	k_Y	7.029	8.579	9.21
Rate factor of the kinematic hardening	C_1	20.12	20.524	14.98
	C_2	30.48	10.163	33.94
Maximum of the kinematic hardening	a_1	13.58	100.296	105.11
	a_2	39.25	48.577	20.02

behavior with or without plastic plateau can be precisely described, which embodies the inherent consistency between the monotonic and cyclic behaviors in the framework of proposed model. However, this feature would not be incorporated in the two existing models that might lead to less accuracy of the prediction than those derived from the new model. In addition, it is noted that the hardening behavior in re-yielding stage and subsequent hardening stagnation can be also depicted with satisfying accuracy, which validates the effectiveness of the mathematically improved evolution rule of the boundary surface. For the results of YU model, it could be noticed that this model could partially describe the basic features of the hardening stagnation dependent on the memory effect but not obtain comparably precise hardening rate in the re-yielding stage, which might result from the monotonic testing data potentially affecting the calibration results of re-yielding rate factor. Meanwhile, the classical Chaboche model fails to describe such phenomenon due to the disregard of memory effect in its original version. Moreover, in the proposed model, it has also been taken in account that the temporary contraction of boundary surface and reduced re-yielding rate after intermediately reverse plastic deformation. These two phenomena can be significantly observed in the case SP-02 as well as SP-07, which is the main purpose for selecting them as the representative loading protocols. The corresponding simulation results manifest that the new evolution function with respect to the normalized plastic internal variable for current plastic status can successfully describe these hysteretic behaviors. However, either the YU or the Chaboche model produce an overestimated result of the predicted stress in the smaller strain amplitude. Moreover, remark that the case SP-09 for Q345/Q420 is the random loading protocol that can be regarded as the integration of possible hysteretic characteristics without regularly arranged patterns. The remarkable agreement with testing data of the random loading scheme suggests the validation of proposed model in predicting the stress-strain response in irregular loading history.

In order to quantify the accuracy of the simulation results based on these three models, an index for the error evaluation is employed to assess the effectiveness of different models in predicting the stress-strain response under various loading schemes. Firstly, for any concerned loading case, it can be readily to obtain the relative error E_i at specific stress point $\sigma_{\text{test},i}$ based on the simulation as well as the testing results, as given by the Eq. (56).

$$E_i = \frac{|\sigma_{\text{model},i} - \sigma_{\text{test},i}|}{|\sigma_{\text{test},i}|} \cdot 100\% \tag{56}$$

By sorting the entire relative error values, we can acquire a specific value $E_{0.955}$ which there is totally 95.5% of data points whose corresponding relative error E_i are less than. Therefore, this index $E_{0.955}$ can be regarded as the relative error index with 95.5% certainty. Unlike the conventional statistic indices represented by the average value, this error index could be employed to quantity the accuracy of certain models as well as reduce the influence resulting from some abnormal testing data

at low stress level due to measuring error. The below-presented Fig. 13 demonstrates the quantified error evaluation of the simulation results based on three constitutive models, including proposed model, YU model as well as Chaboche model, upon three different steels with various yielding strength. It is noted that the proposed model manifests the significantly better prediction results rather than the other two models, which could be indicated by the comparably low error index $E_{0.955}$ whose maximum is less than 11% in any loading cases of three different steel materials. In particular, for the random loading schemes in Q345 and Q420, these data are crucial to examine the generalization ability of concerned model and also to investigate its feasibility in the prediction of the structural response under irregular seismic action. These corresponding error indices suggest that the proposed model is capable to obtain the more accurate stress-strain response under random loading history, with the 7.1% error index for Q345 and 9.8% for Q420, compared with the higher error indices of the YU model and Chaboche model in such loading scheme. The main reason for the improvement of prediction is that the proposed model is able to incorporate more potential cyclic behaviors than the other conventional models. For instance, the large error produced by the Chaboche model is due to its lack of capacity in description of strain range dependence effect. It will lead to the misprediction of the shape of hysteretic loops in large strain amplitude, as shown in Fig. 10., once using the constant parameters consistent with data in small strain amplitude. Compared with the results of Chaboche model, the YU model can produce better prediction since the memory surface is included for the strain range dependence, as presented in Fig. 10. SP-01. However, both of them will still not make satisfying prediction under descending strain controlled test, as illustrated in Fig. 10. SP-02 In contrast, the proposed model can produce more better prediction since three major mechanisms related to the change of stress boundary surface are considered within the basic framework, especially including the temporary contraction of stress boundary surface due to intermediate reverse strain as indicated in Fig. 10. SP-02 of proposed model. Upon the error analysis, it could be concluded that the testing data from three typical loading cases, namely the uniaxial monotonic tensile test, the multi-level increasing as well as decreasing strain-amplitude controlled test, are sufficient to calibrate the appropriate material parameters of proposed model to acquire the stress-strain response under irregular seismic action with satisfying accuracy.

5. Conclusions

With the collective considerations of various hardening behavior of common steels, this paper presents a new model in order to incorporate these phenomena and to address the problems with the accuracy as well as convergence in numerical process involved with the existing models. The primary improvements of proposed model can be summarized as the following statements:

(1) A new evolution rule of backstress is developed to describe the work-hardening stagnation. It originates from the concept of virtual boundary surface and is formulated as the combination of
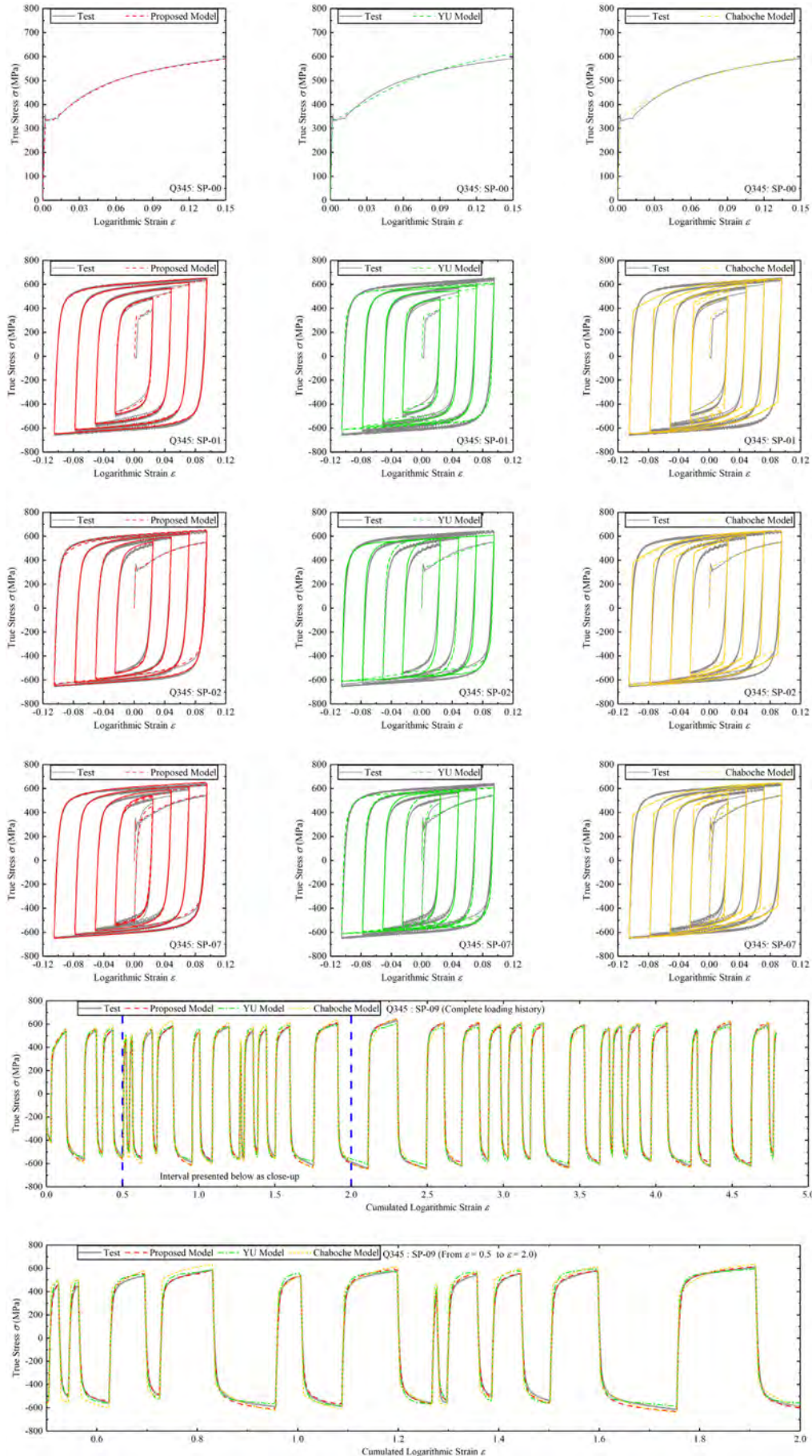
Fig. 10. Simulation results based on three models under selected loading protocols compared with Q345 steel material testing results.

14
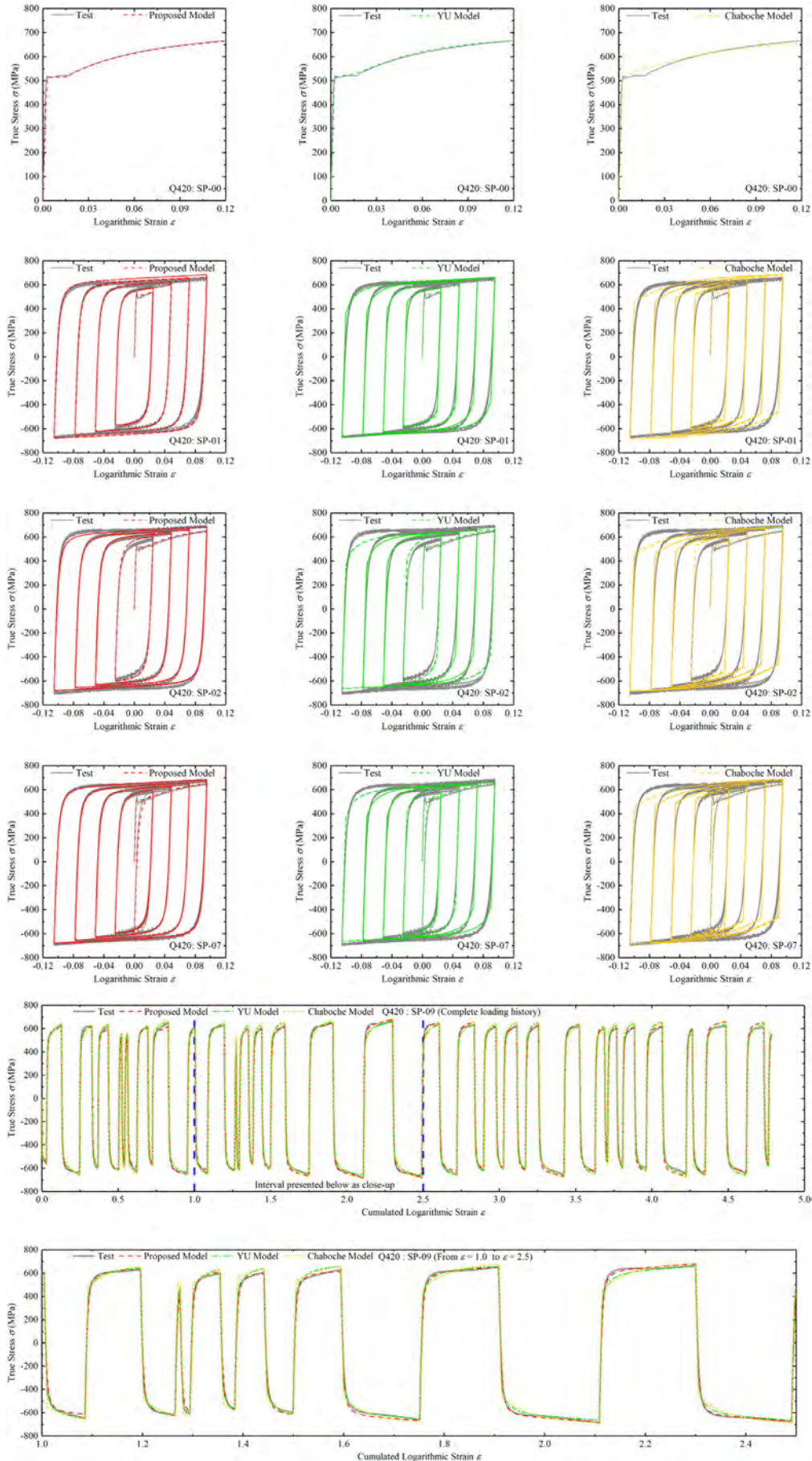
Fig. 11. Simulation results based on three models under selected loading protocols compared with Q420 steel material testing results.
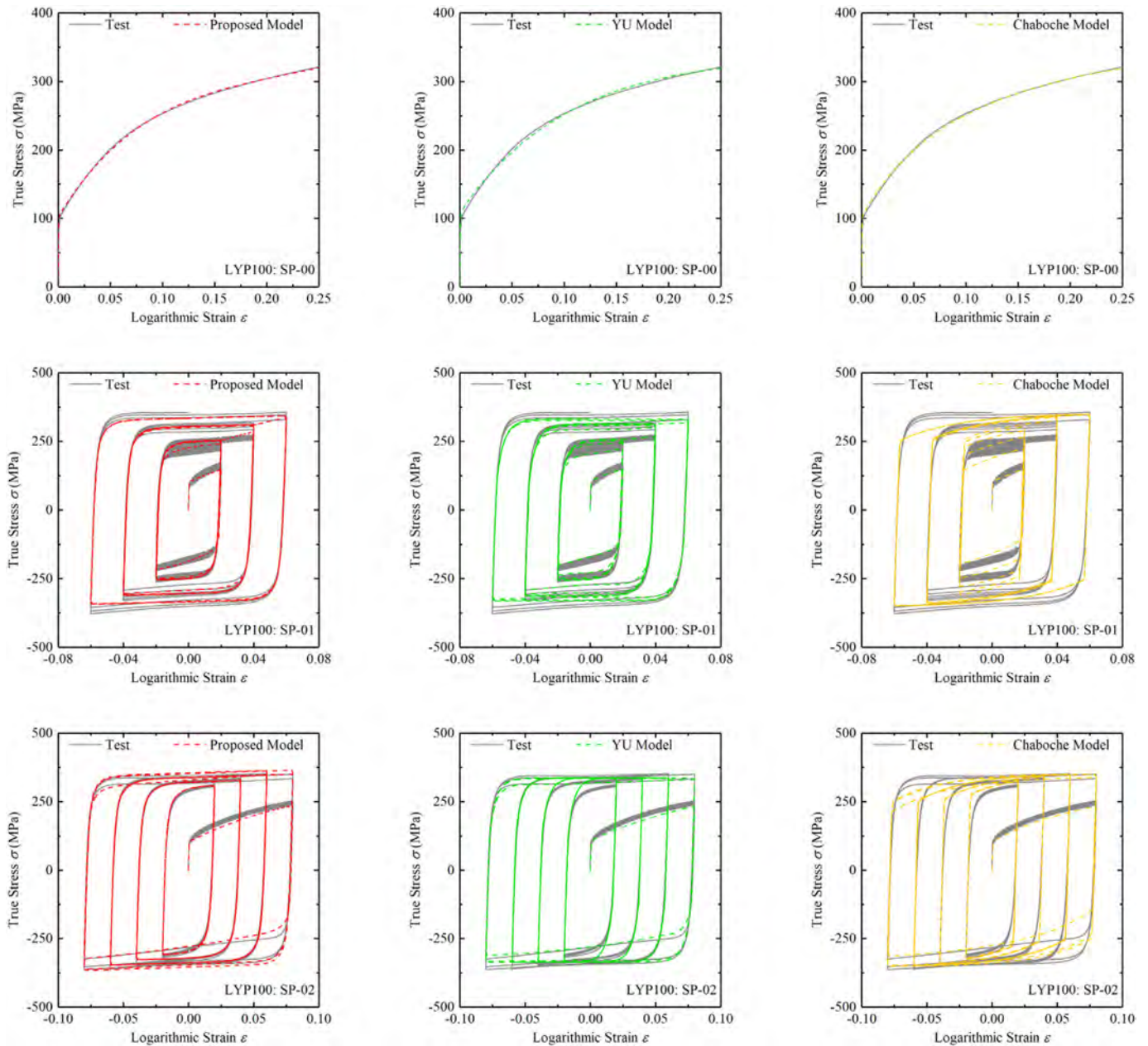
Fig. 12. Simulation results based on three models under selected loading protocols compared with LYP100 steel material testing results.

several superposed components, which leads to an explicit discrete update formulation and fundamentally eliminate the convergence problems potentially encountered in YU model.

(2) This model considers the memory effects in strain space. The generalized evolution rule of memory surface is employed and transformed to the discrete update formulations that are second-order continuous in order to improve the convergence in numerical procedure.

(3) The evolution rule of boundary surface determines the value of peak stress in the stagnation status. In this model, the radius of boundary surface is assumed as the combination of three separated parts, which refer to the expansion of boundary surface induced by the increasing memorized strain range, by the accumulated plastic strain in fixed memorized strain range, and the temporary contraction after intermediately reverse plastic deformation.

(4) The term referring to the boundary surface expansion induced by the increasing memorized strain range can be explicitly

determined by the monotonic tensile test. These involved formulas ensure fundamentally the inherent consistency between monotonic and cyclic behavior so that it can lead to a perfect reproduction of the monotonic stress-strain relationship, regardless of the change of parameters involved with cyclic behaviors.

(5) Another term, indicating the boundary surface expansion induced only by accumulated plastic strain, is defined as the variable that can only be altered in fixed memorized strain range. Based on this assumption, a new incremental plastic variable is defined as the difference of the increment of accumulated plastic strain and the memorized strain range. This variable will become positive only if the cyclic loading is imposed within the fixed memorized strain range, so that it can determine the boundary surface expansion induced by accumulated plastic strain.

(6) A new normalized plastic internal variable is defined to quantify the current plastic status compared with the memorized stain range in the whole loading history. With respect to this newly proposed internal variable, it is possible to evaluate the
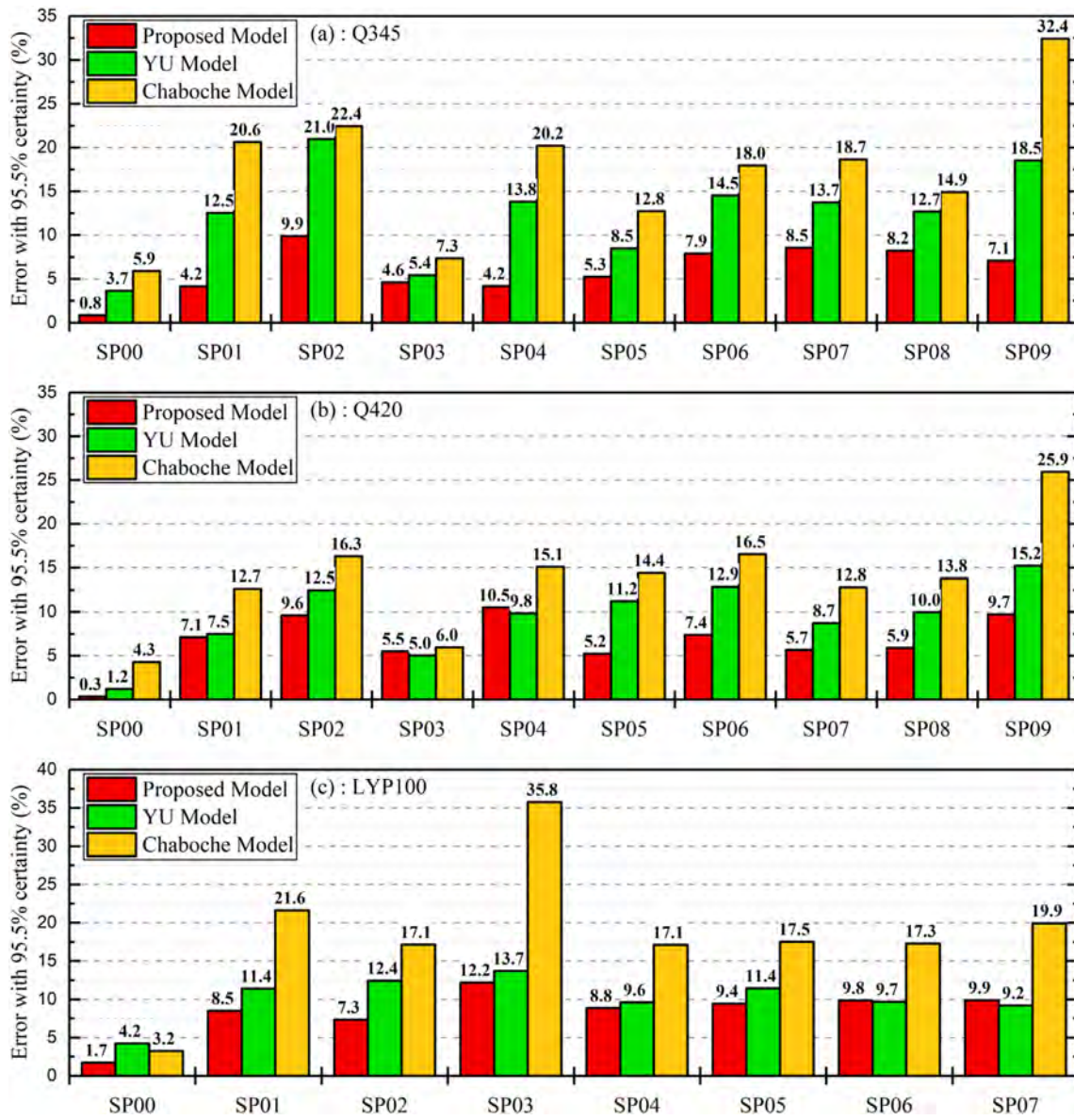
Fig. 13. Relative error indices of the simulations based on three models.

dependence of the temporary contraction of boundary surface as well as the reduction of re-yielding rate on the current plastic status when the reverse plastic deformation is applied.

(7) An additional consideration of the dependence of the elastic region size on the memorized strain range is incorporated in this model, in accordance with the involved studies suggesting that the yield surface might be altered with respect to the plastic history.

All these features are formulated by the mutual independent equations that describe the corresponding plastic behaviors, which facilitates the calibration process. Through the comparison of the simulation results and the experimental data, it can be concluded that these hardening behaviors can be precisely described by proposed model. Moreover, the remarkable agreement with experimental results under random loading schemes can validate its capacity of predicting the stress-strain response of different structural steels under irregular actions.

Author statement

Manuscript title: A constitutive model for various structural steels considering shared hysteretic behaviors.

Declaration of Competing Interest

The authors declare that they have no known competing financial interests or personal relationships that could have appeared to influence the work reported in this paper.

The authors declare the following financial interests/personal relationships which may be considered as potential competing interests:

Acknowledgement

References

[1] G. Shi, F. Hu, Y. Shi, Recent research advances of high strength steel structures and codification of design specification in China, Intern. J. Steel Struct. 14 (2015) 873–887.

[2] E. Saeki, M. Sugisawa, T. Yamaguchi, A. Wada, Mechanical properties of low yield point steels, J. Mater. Civ. Eng. 10 (1998) 143–152.

[3] J. Cao, W. Lee, H.S. Cheng, M. Seniw, H.-P. Wang, K. Chung, Experimental and numerical investigation of combined isotropic-kinematic hardening behavior of sheet metals, Int. J. Plast. 25 (2009) 942–972.

[4] P. Dusicka, A.M. Itani, I.G. Buckle, Cyclic response of plate steels under large inelastic strains, J. Constr. Steel Res. 63 (2007) 156–164.

[5] Q. He, Y. Chen, K. Ke, M.C.H. Yam, W. Wang, Experiment and constitutive modeling on cyclic plasticity behavior of LYP100 under large strain range, Constr. Build. Mater. 202 (2019) 507–521.

[6] F. Hu, G. Shi, Y. Shi, Constitutive model for full-range elasto-plastic behavior of structural steels with yield plateau: calibration and validation, Eng. Struct. 118 (2016) 210–227.

[7] M. Nakashima, Strain-hardening behavior of shear panels made of low-yield steel. I: test, J. Struct. Eng. 121 (1995) 1742–1749.

[8] N. Nishimura, K. Ono, T. Ikeuchi, A constitutive equation for structural steels based on a monotonic loading curve under cyclic loading, Doboku Gakkai Ronbunshu 1995 (1995) 27–38.

[9] N. Nishimura, K. Ono, T. Ikeuchi, T. Shinke, Experimental investigation on hysteretic behavior of structural steels in plastic range, Kou Kouzou Rombunshuu 1 (1994) 173–182.

[10] C.P. Shen, I.H. Mamaghani, E. Mizuno, T. Usami, Cyclic behavior of structural steels. II: theory, J. Eng. Mech. 121 (1995) 1165–1172.

[11] G. Shi, M. Wang, Y. Bai, F. Wang, Y. Shi, Y. Wang, Experimental and modeling study of high-strength structural steel under cyclic loading, Eng. Struct. 37 (2012) 1–13.

[12] Y. Shi, M. Wang, Y. Wang, Experimental and constitutive model study of structural steel under cyclic loading, J. Constr. Steel Res. 67 (2011) 1185–1197.

[13] A. Ucak, P. Tsopelas, Constitutive model for cyclic response of structural steels with yield plateau, J. Struct. Eng. 137 (2010) 195–206.

[14] M. Wang, L.A. Fahnestock, F. Qian, W. Yang, Experimental cyclic behavior and constitutive modeling of low yield point steels, Constr. Build. Mater. 131 (2017) 696–712.

[15] L. Xu, X. Nie, J. Fan, M. Tao, R. Ding, Cyclic hardening and softening behavior of the low yield point steel BLY160: experimental response and constitutive modeling, Int. J. Plast. 78 (2016) 44–63.

[16] F. Yoshida, T. Uemori, A model of large-strain cyclic plasticity describing the Bauschinger effect and workhardening stagnation, Int. J. Plast. 18 (2002) 661–686.

[17] F. Zhou, Y. Chen, Q. Wu, Dependence of the cyclic response of structural steel on loading history under large inelastic strains, J. Constr. Steel Res. 104 (2015) 64–73.

[18] W. Prager, Recent developments in the mathematical theory of plasticity, J. Appl. Phys. 20 (1949) 235–241.

[19] P.J. Armstrong, C. Frederick, A Mathematical Representation of the Multiaxial Bauschinger Effect, Central Electricity Generating Board [and] Berkeley Nuclear Laboratories, 1966 RD/B/N731.

[20] W.D. Iwan, On a class of models for the yielding behavior of continuous and composite systems, J. Appl. Mech. 34 (1967) 612–617.

[21] Z. Mroz, On the description of anisotropic workhardening, J. Mech. Phys. Solids 15 (1967) 163–175.

[22] Y.F. Dafalias, E.P. Popov, A model of nonlinearly hardening materials for complex loading, Acta Mech. 21 (1975) 173–192.

[23] R. Krieg, A practical two surface plasticity theory, J. Appl. Mech. 42 (1975) 641–646.

[24] E. Popov, Plastic Internal Variables Formalism of Cyclic Plasticity, Annual Meeting, New York NY December 1976 10.

[25] J. Chaboche, K.D. Van, G. Cordier, Modelization of the strain memory effect on the cyclic hardening of 316 stainless steel, Proc SMIRT_5 Conf Berlin 1979, L11/3, 1, , 1979.

[26] J. Chaboche, G. Rousselier, On the plastic and viscoplastic constitutive equations—part I: rules developed with internal variable concept, J. Press. Vessel. Technol. 105 (1983) 153–158.

[27] J. Chaboche, G. Rousselier, On the plastic and viscoplastic constitutive equations—part II: application of internal variable concepts to the 316 stainless steel, J. Press. Vessel. Technol. 105 (1983) 159–164.

[28] J.-L. Chaboche, Time-independent constitutive theories for cyclic plasticity, Int. J. Plast. 2 (1986) 149–188.

[29] J.-L. Chaboche, On some modifications of kinematic hardening to improve the description of ratchetting effects, Int. J. Plast. 7 (1991) 661–678.

[30] J. Chaboche, O. Jung, Application of a kinematic hardening viscoplasticity model with thresholds to the residual stress relaxation, Int. J. Plast. 13 (1997) 785–807.

[31] J.L. Chaboche, A review of some plasticity and viscoplasticity constitutive theories, Int. J. Plast. 24 (2008) 1642–1693.

[32] H.P. Feigenbaum, Y.F. Dafalias, Directional distortional hardening in metal plasticity within thermodynamics, Int. J. Solids Struct. 44 (2007) 7526–7542.

[33] H.P. Feigenbaum, Y.F. Dafalias, Simple model for directional distortional hardening in metal plasticity within thermodynamics, J. Eng. Mech. 134 (2008) 730–738.

[34] H.P. Feigenbaum, J. Dugdale, Y.F. Dafalias, K.I. Kourousis, J. Plesek, Multiaxial ratcheting with advanced kinematic and directional distortional hardening rules, Int. J. Solids Struct. 49 (2012) 3063–3076.

[35] M. Abdel-Karim, Modified kinematic hardening rules for simulations of ratchetting, Int. J. Plast. 25 (2009) 1560–1587.

[36] M. Abdel-Karim, An evaluation for several kinematic hardening rules on prediction of multiaxial stress-controlled ratchetting, Int. J. Plast. 26 (2010) 711–730.

[37] M. Abdel-Karim, N. Ohno, Kinematic hardening model suitable for ratchetting with steady-state, Int. J. Plast. 16 (2000) 225–240.

[38] N. Ohno, M. Abdel-Karim, Uniaxial ratcheting of 316FR steel at room temperature—part II: constitutive modeling and simulation, J. Eng. Mater. Technol. 122 (2000) 35.

[39] J.L. Chaboche, A. Gaubert, P. Kanouté, A. Longuet, F. Azzouz, M. Mazière, Viscoplastic constitutive equations of combustion chamber materials including cyclic hardening and dynamic strain aging, Int. J. Plast. 46 (2013) 1–22.

[40] J.L. Chaboche, P. Kanouté, F. Azzouz, Cyclic inelastic constitutive equations and their impact on the fatigue life predictions, Int. J. Plast. 35 (2012) 44–66.

[41] Y.F. Dafalias, H.P. Feigenbaum, Biaxial ratcheting with novel variations of kinematic hardening, Int. J. Plast. 27 (2011) 479–491.

[42] T. Hassan, L. Taleb, S. Krishna, Influence of non-proportional loading on ratcheting responses and simulations by two recent cyclic plasticity models, Int. J. Plast. 24 (2008) 1863–1889.

[43] S. Krishna, T. Hassan, I. Ben Naceur, K. Saï, G. Cailletaud, Macro versus micro-scale constitutive models in simulating proportional and nonproportional cyclic and ratcheting responses of stainless steel 304, Int. J. Plast. 25 (2009) 1910–1949.

[44] F. Yoshida, Y. Kaneda, S. Yamamoto, A plasticity model describing yield-point phenomena of steels and its application to FE simulation of temper rolling, Int. J. Plast. 24 (2008) 1792–1818.

[45] D. Yu, G. Chen, W. Yu, D. Li, X. Chen, Visco-plastic constitutive modeling on Ohno–Wang kinematic hardening rule for uniaxial ratcheting behavior of Z2CND18.12N steel, Int. J. Plast. 28 (2012) 88–101.

[46] D. Yu, X. Chen, W. Yu, G. Chen, Thermo-viscoplastic modeling incorporating dynamic strain aging effect on the uniaxial behavior of Z2CND18.12N stainless steel, Int. J. Plast. 37 (2012) 119–139.

[47] Y. Zhu, G. Kang, Q. Kan, O.T. Bruhns, Logarithmic stress rate based constitutive model for cyclic loading in finite plasticity, Int. J. Plast. 54 (2014) 34–55.

[48] X.-F. Xie, W. Jiang, J. Chen, X. Zhang, S.-T. Tu, Cyclic hardening/softening behavior of 316L stainless steel at elevated temperature including strain-rate and strain-range dependence: experimental and damage-coupled constitutive modeling, Int. J. Plast. 114 (2019) 196–214.

[49] Y. Zhu, G. Kang, C. Yu, A finite cyclic elasto-plastic constitutive model to improve the description of cyclic stress-strain hysteresis loops, Int. J. Plast. 95 (2017) 191–215.

[50] G. Kang, N. Ohno, A. Nebu, Constitutive modeling of strain range dependent cyclic hardening, Int. J. Plast. 19 (2003) 1801–1819.

[51] N. Ohno, J.-D. Wang, Kinematic hardening rules with critical state of dynamic recovery, part I: formulation and basic features for ratchetting behavior, Int. J. Plast. 9 (1993) 375–390.

[52] N. Ohno, J.D. Wang, Transformation of a nonlinear kinematic hardening rule to a multisurface form under isothermal and nonisothermal conditions, Int. J. Plast. 7 (1991) 879–891.

[53] N. Ohno, A constitutive model of cyclic plasticity with a nonhardening strain region, J. Appl. Mech. 49 (1982) 721–727.

[54] R. Ahmed, P.R. Barrett, T. Hassan, Unified viscoplasticity modeling for isothermal low-cycle fatigue and fatigue-creep stress–strain responses of Haynes 230, Int. J. Solids Struct. 88–89 (2016)131–45.

[55] D. Nouailhas, G. Cailletaud, H. Policella, D. Marquis, J. Dufailly, H. Lieurade, et al., On the description of cyclic hardening and initial cold working, Eng. Fract. Mech. 21 (1985) 887–895.

[56] L. Taleb, G. Cailletaud, An updated version of the multimechanism model for cyclic plasticity, Int. J. Plast. 26 (2010) 859–874.

[57] J. Zhou, Z. Sun, P. Kanouté, D. Retraint, Experimental analysis and constitutive modelling of cyclic behaviour of 316L steels including hardening/softening and strain range memory effect in LCF regime, Int. J. Plast. 107 (2018) 54–78.

[58] FEMA P, Quantification of Building Seismic Performance Factors, Washington, DC, 2009.

[59] F. Hu, G. Shi, Y. Shi, Constitutive model for full-range elasto-plastic behavior of structural steels with yield plateau: formulation and implementation, Eng. Struct. 171 (2018) 1059–1070.

[60] V. Abaqus, 6.14 Documentation, 651, Dassault Systemes Simulia Corporation, 2014 6.2.